Repair of a Model Masonry Arch Bridge using FRP

Repair of a Model Masonry Arch Bridge using FRP

Y. Tao, J.F. Chen and T.J. Stratford

Institute for Infrastructure and Environment
Joint Research Institute for Civil and Environmental Engineering
The University of Edinburgh, Scotland, UK

ABSTRACT

Masonry arch bridges form a significant proportion of the road and rail infrastructure in the UK. As the majority of these were constructed in the 19th century or earlier, most of them were not designed originally to carry the loads imposed on them by modern traffic. Many existing masonry arch bridges have therefore been damaged and may require repair or strengthening. This paper presents a laboratory test on a single ring large scale model masonry arch bridge. The bridge was loaded close to collapse and so that cracks formed to simulate damage. The bridge was then repaired by bonding fibre-reinforced polymer (FRP) onto its intrados, and tested to destruction. The results show that the FRP strengthening is an effective technique for increasing the load capacity of the bridge using a small amount of FRP.

INTRODUCTION

Masonry arch bridges make up a significant proportion of the transport infrastructure in many countries. Most of these arch bridges are historical constructions and were not initially designed to carry modern traffic loads, which can result in damage to them. In order to extend the life of these structures, fibre reinforced polymer (FRP) composite repair or strengthening techniques have been investigated to reinstate or enhance the performance of masonry arch bridges [1, 2, 3, 4].

This paper describes experimental research conducted on the one-third scale, two-span masonry arch bridge model shown in Figures 1 and 2. The arches were tested before and after being repaired using FRP. The focus of the current paper is the tests on the southern arch. The tests on the northern arch are presented elsewhere [5].

EXPERIMENTAL INVESTIGATION

Tests Prior to Repair

The arches were constructed from a single ring of concrete bricks, with the dimensions shown in Figure 1. Rigid abutments were provided to either ends using steelwork, and the abutments and side of the bridge were clad in timber to contain sand fill.

Prior to the FRP repair, each of the arches was loaded in turn to establish a four-hinge mechanism. A line load was applied at the quarter span position (shown in Figures 1 and 3a), as this is usually the worst loading position [6]. The load was applied using hydraulic jacks that acted upon a steel spreader beam and timber spreader plate. Load cells were used to measure the applied load and seven displacement transducers (D_{S1}~D_{S5} and D_{N1}~D_{N2}) were installed beneath the arches to measure the radial displacement (Figure 3). Each arch was loaded until the four-hinge mechanism was fully developed and the load capacity of the unstrengthened arch was estimated to be almost reached.

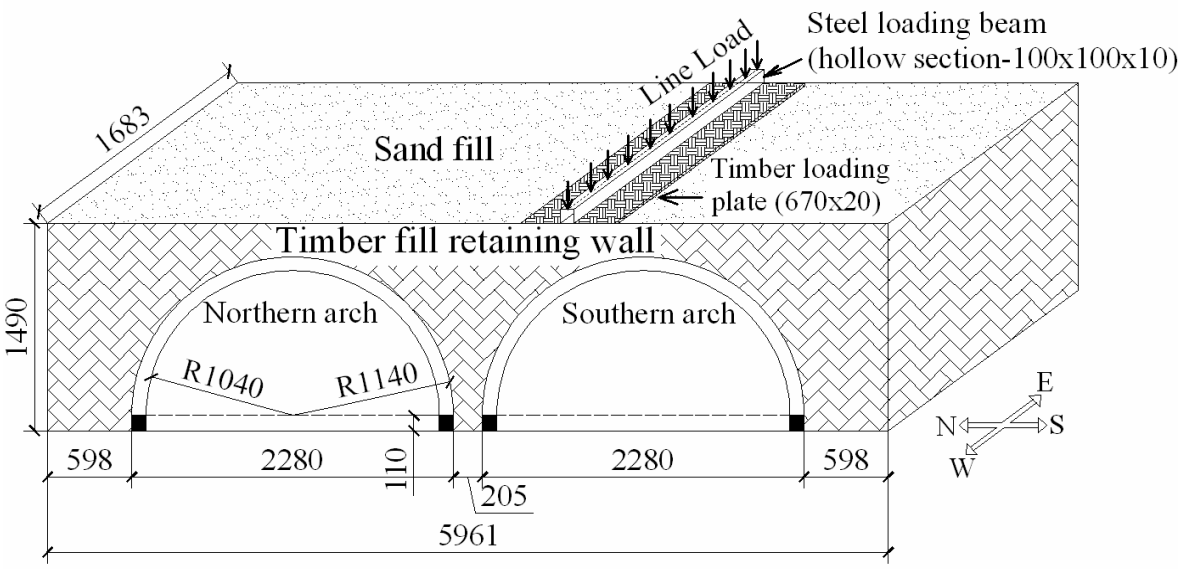

Figure 1. Overview of the arch bridge model (mm)

Test upon the Repaired Southern Arch

The arches were repaired using pultruded carbon FRP (CFRP) plates, which were bonded to the intrados of the arches as shown in Figures 2 and 3. Three CFRP plates were applied to the northern arch, and six to the southern arch, evenly distributed across the width of the arch (as shown in Figure 3b for the southern arch). The CFRP plates had a cross-section of 100×1.4mm, a Young's modulus of 170GPa and tensile strength of 3100MPa (based upon the manufacturer's values).

The surface of the masonry was prepared by grinding to remove the irregularities and cleaning by wire brush, vacuum and solvent treatment. An epoxy primer was applied before

bonding the CFRP plates to the masonry using a two-part ambient cure epoxy adhesive with about 2mm thickness. Temporary support was provided until the adhesive cured.

In addition to the instrumentation used for the test prior to repair, 5 PI gauges were used to measure the crack opening widths on either side of the arches and 25 strain gauges (S_{S1-1} to S_{S6-2} in south arch) were applied along the centre lines of the FRP plates, as shown in Figure 3. The arches were again loaded at the quarter span.

Figure 2. The western elevation of the arches after repair with CFRP

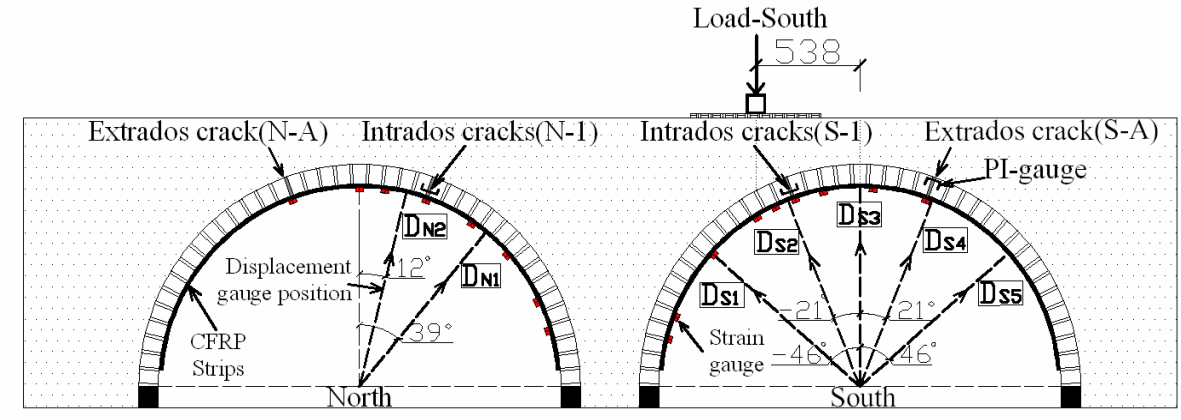

(a) Western elevation

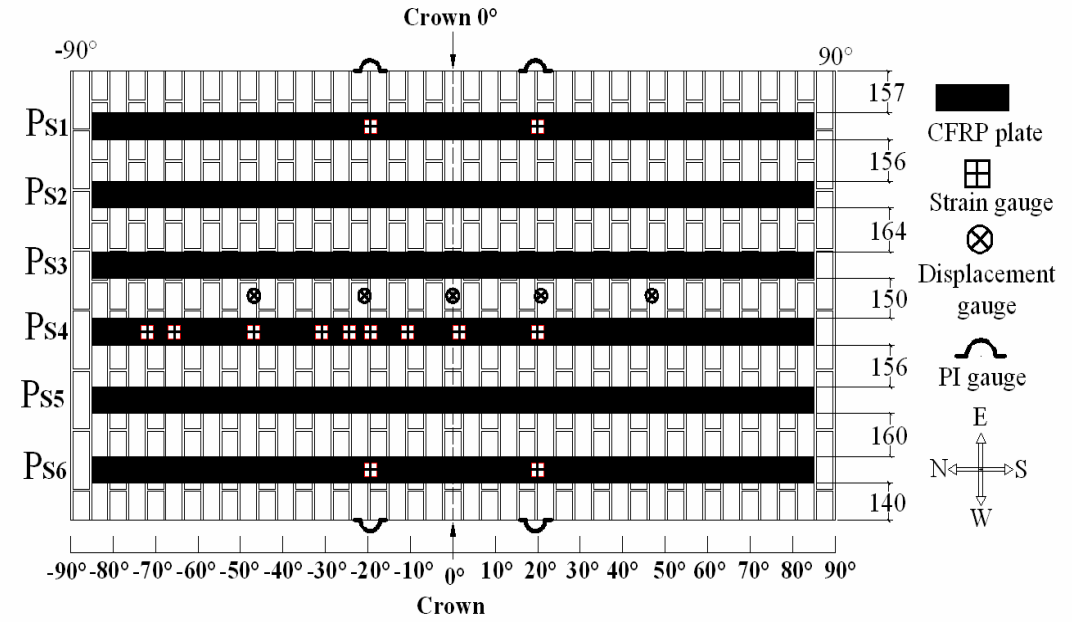

(b) Developed length plan view of the southern arch (mm)

Figure 3. Positions of CFRP plates and instrumentation

FAILURE MECHANISM OF THE REPAIRED ARCH

Previous work has established that there are four main failure mechanisms for FRP-strengthened masonry arches [1, 2, 3, 4, 7, 8]:

a) crushing of the masonry;
b) tensile rupture of the FRP;
c) debonding of the FRP along the adhesive joint due to rotational opening of a crack in the masonry (flexural cracking); and
d) debonding of the FRP due to shearing of the masonry joints

During the test on the repaired southern arch, failure occurred in three stages, through a combination of mechanisms (c) and (d).

The initial FRP debonding failure occurred at the intrados hinge beneath the loading point at a load 250kN (Figure 4). The opening of the intrados crack (S-1) required high shear stress to be transferred across the adhesive, resulting in debonding of plate P_{S2} from the masonry. At this stage, the bond of the other five CFRP plates remained intact.

Additional opening of the cracks occurred as the load continued to increase by a small amount. This increased the bond stresses between the CFRP and the masonry, and consequently led to extensive partial debonding of all the CFRP plates. The final debonding

event was sudden and brittle. It was not possible to distinguish the sequence between the debonding of individual plates.

The type of masonry cracking and debonding varied across the width of the bridge as shown in Figure 5 where sections through the arch along each of the CFRP plates are shown. A new intrados crack (S-2) opened two bricks away from the original crack (S-1) at the east side of the bridge as shown in Figure 6. This new crack certainly crossed CFRP plate P_{S1} and P_{S2}, but it was not clear from photographs (direct observation underneath the bridge was not possible due to health and safety concerns) how far it penetrated into the central portion of the arch (P_{S3} and P_{S4}), but it was clear that this new crack did not extend to the west side of the bridge so it did not cross CFRP plate P_{s5} and P_{s6}. At the west side of the bridge, a mixture of rotational opening and shear occurred at intrados crack (S-1) as shown in Figure 7.

Figures 5 and 8 show the extent of debonding of each CFRP plate. Debonding of plates P_{S1}, P_{S2}, P_{S3} and P_{S4} was clearly due to rotational opening of the intrados crack (Figures 5a, b, c and d). The debonding of plate P_{S6} also appears to have been dominated by rotational opening of the intrados crack, as the debonded region bridges the crack (Figure 5f). Plate P_{S5}, however, appears to have been dominated by shearing of the masonry joint, accompanied by peel debonding that started at the intrados crack (Figure 5e).

In all cases, separation of the CFRP from the masonry occurred slightly within the masonry, and left a thin layer of brick bonded to the plate to either side of the hinge. Further back from the hinge, however, the separation occurred within the laminate, leaving exposed fibres (Figure 9).

The load on the bridge was dropped significantly after the partial debonding of all the FRP plates. At this stage in the test, the arch was completely unloaded so that the instrumentation could be removed. The southern arch was then reloaded to collapse to determine the residual strength after debonding. The final stage of failure was a four-pin collapse of the arch.

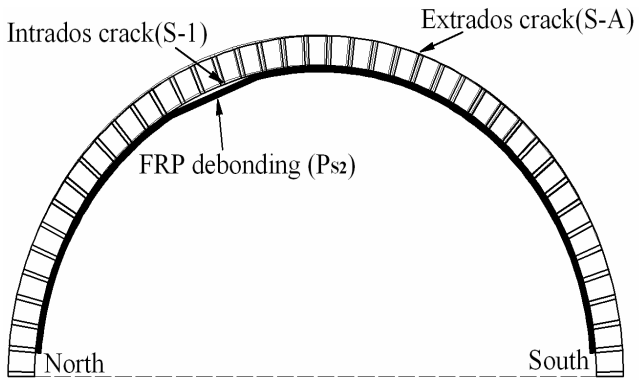

Figure 4. Plate P_{S2} on the southern arch after first debonding.

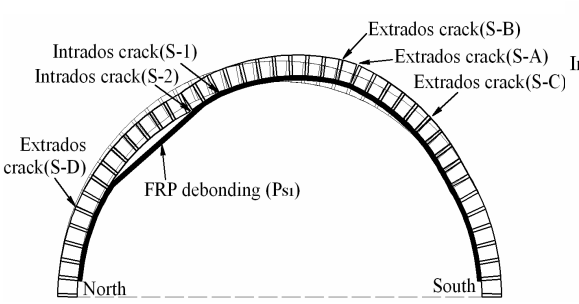

(a) Plate P_{S1}

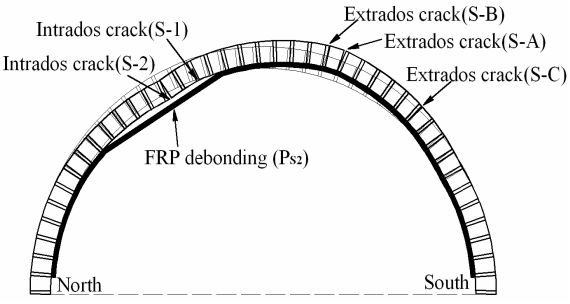

(b) Plate P_{S2}

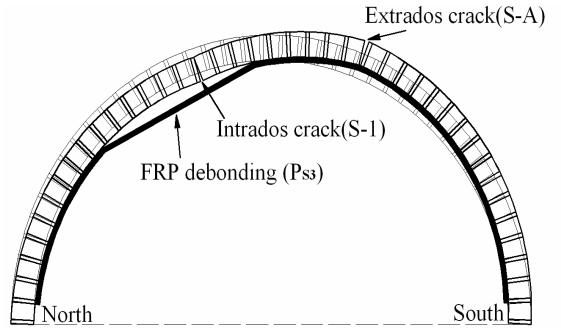

(c) Plate P_{S3}

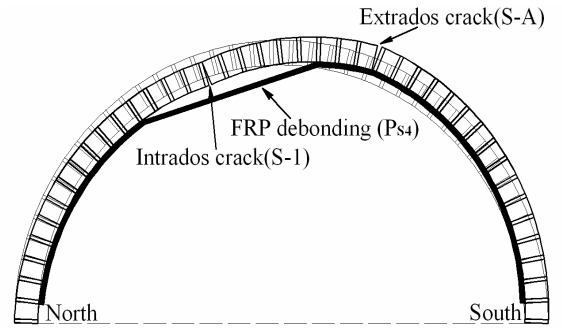

(d) Plate P_{S4}

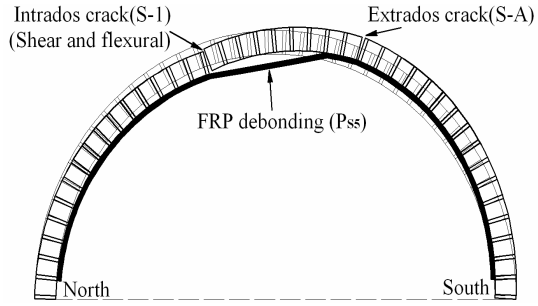

(e) Plate P_{S5}

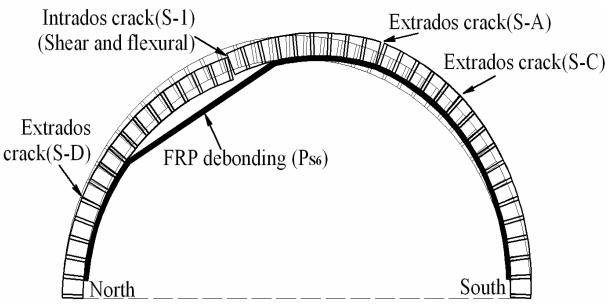

(f) Plate P_{S6}

Figure 5. Deformed shape of the southern arch and position of FRP after final debonding, shown along each CFRP plate section and viewed from the west.

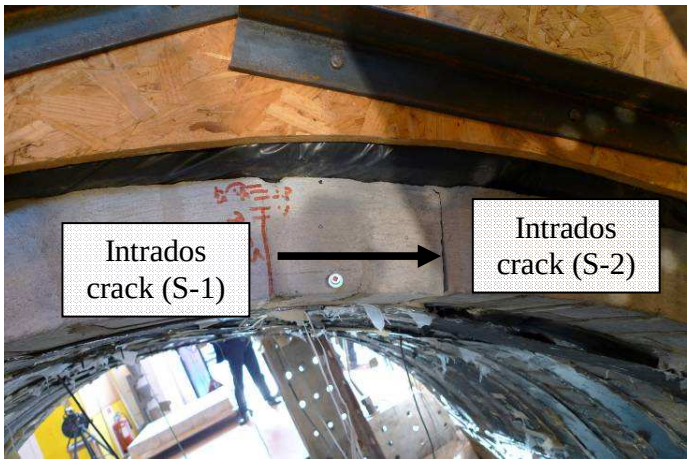

Figure 6. Development of second intrados crack near the loading position - viewed from the west

Figure 7. Mixed shear and flexural cracking failure at intrados crack (S-1) - viewed from the east

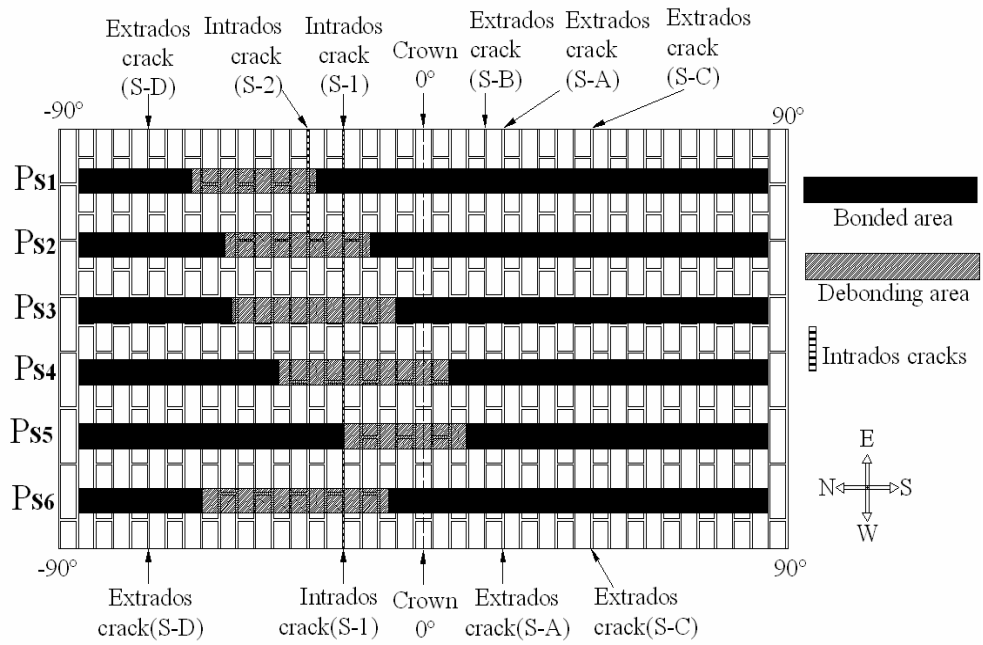

Figure 8. Plan view along the developed length of the southern arch after failure, showing the location of cracks and extent of debonding

Figure 9. Debonding of the CFRP plate within the laminate, plate P_{S4}

LOAD-DISPLACEMENT RESPONSE OF THE ARCH

Figure 10 shows the load-displacement response of both the original and the repaired arches, recorded by each of the seven displacement gauges (Figure 3).

The original arch (prior to FRP repair) was dominated by opening of the four hinge mechanism cracks. The displacement significantly increased once the mechanism established at around 39kN. The small crown displacement (D_{S3}) and the large displacements in opposite directions at D_{S2} and D_{S4}, and the smaller displacements at D_{S1} and D_{S5} correspond to the four-hinge mechanism. Negligible displacement were observed in the adjacent northern arch (D_{N1}), indicating that only small interaction exists between the two arches. Note that large residual displacements remained after unloading, as the cracks were unable to completely close. The applied load reached up to 49.7kN which was estimated to be very close to the strength of original arch.

The response of the repaired arch is stiffer, as the FRP restricts the opening of the intrados cracks. Consequently, the displacement on the north side (D_{S1}) where the FRP on the intrados restricted the opening of intrados crack, was smaller than on the south side (D_{S5}) where the FRP on the intrados did not restrict the extrados crack. After a load of about 180kN, some fluctuations occurred in the curves probably due to the progressive build up of micro-crack damage in the masonry, nonlinear deformation of masonry under compression at the hinge positions, and softening at the interface between CFRP and masonry. The deformation increased much more rapidly after that due to these nonlinear factors. The first debonding event (Figure 4) was at a load of 250.0kN, giving a drop in the load-deflection response. The capacity of the repaired arch was reached at 253.8kN when all 6 plates debonded (Figure 7), which was 511% greater than the estimated strength of the original arch.

The load dropped to 90.6kN after the debonding of all the 6 CFRP plates. It should be noted that the value of this residual load depends upon the stiffness of the hydraulic loading system. The arch was unloaded, and the instrumentation removed. Large residual deformation after unloading is clearly seen in Figure 10. The arch was reloaded to destruction. The residual strength after FRP debonding failure was determined from this process to be 113.3kN. Note that this residual strength of the FRP repaired arch was still much higher than the strength of the original (un-repaired) arch because the debonding FRP plates formed ties and altered the structural behaviour. The displacement was not recorded during the final loading process because the transducers had been removed.

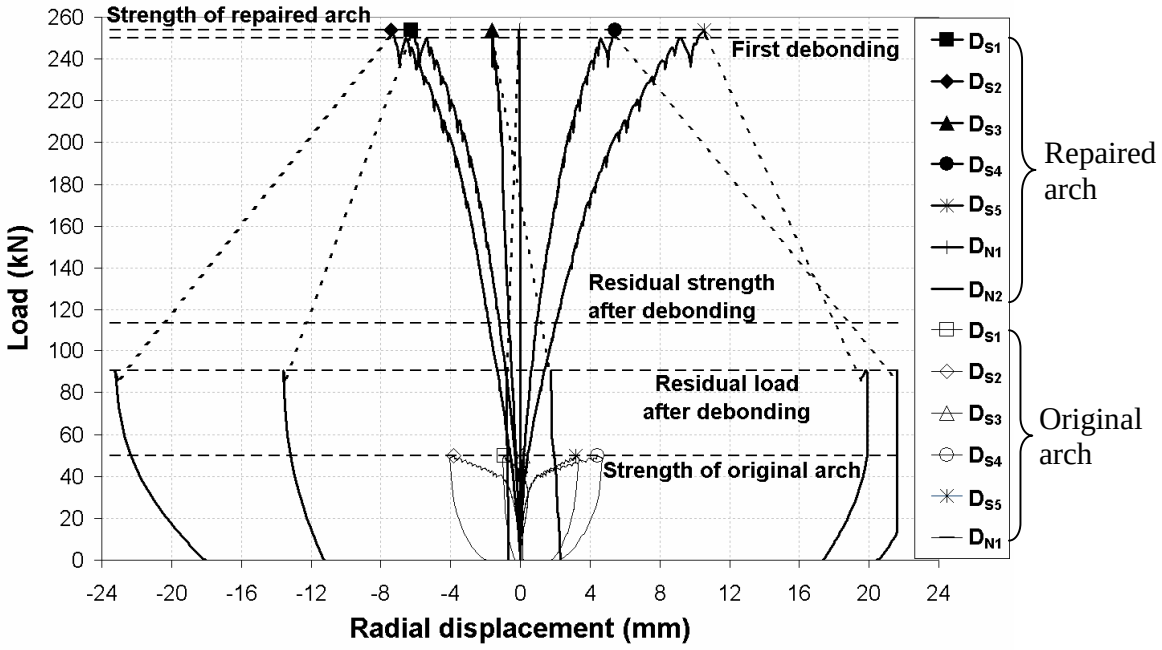

Figure 10. Load vs. radial displacement curves for the southern arch

FRP STRAIN RESPONSE

Figure 11 plots the CFRP strain profiles along plate P_{S4} at different levels of load. This plate failed by debonding at the intrados crack (Figure 5d) in the region between strain gauges S_{S4-4} and S_{S4-8}.

Up to a load of 200kN, the peak strain was at intrados crack (S-1) (gauge S_{S4-6}). The strains decreased to either side of the crack, with compressive strain corresponding to the two extrados crack in the 4 hinge mechanism at S_{S4-1}, S_{S4-2} and S_{S4-9} (Figure 5d).

When the load was greater than 200kN, the location of the maximum strain was shifted from S_{S4-6} to S_{S4-5}. This corresponds to the development of the second intrados crack as discussed above. The magnitude of the strain profile beyond 180kN increases rapidly with load, due to softening of the CFRP-masonry interface, in a similar manner to the load-deflection response.

A sudden increase in strain occurred from 240kN to 250kN, when the first debonding occurred on plate P_{S2}, and load was redistributed onto plate P_{S4}. Between 250kN and 253kN, the strain at gauge S_{S4-5} was constant, but the strain to either side (S_{S4-4} and S_{S4-6}) increased, as the debonded region of CFRP increased away from the hinge zone in the region of intrados cracks (S-1) and (S-2).

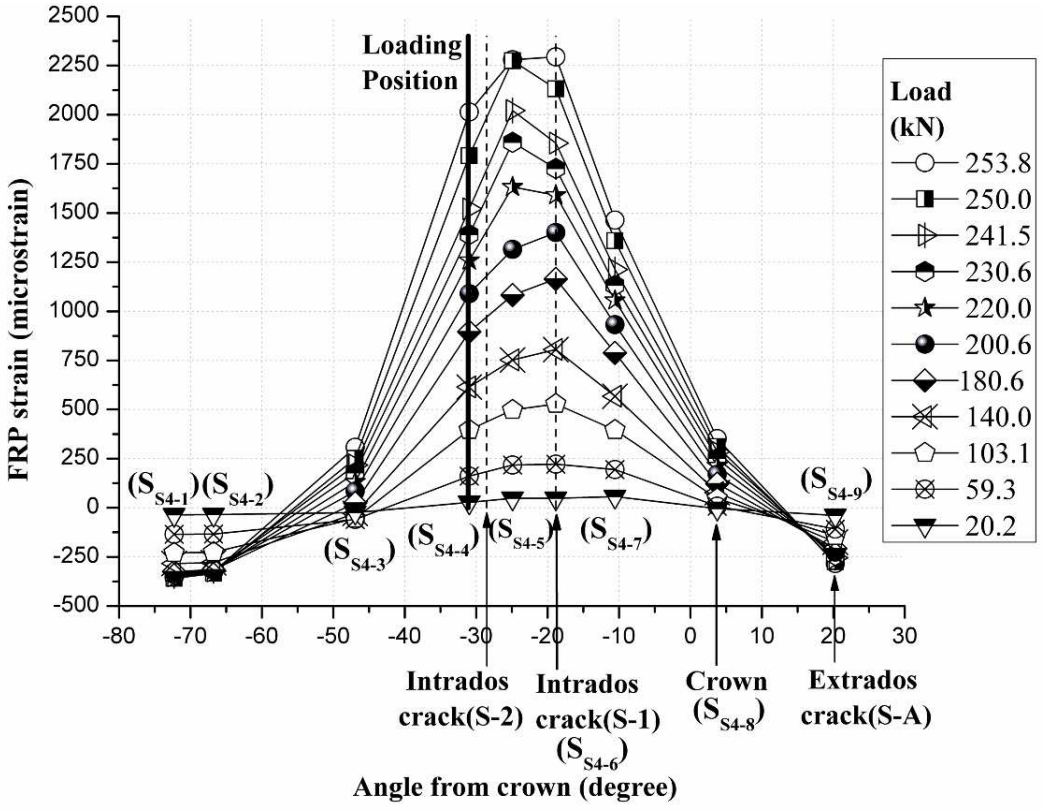

Figure 11. CFRP strain profiles for strain gauges on plate P_{S4}

CONCLUSIONS

This paper has presented the test results from the southern span of a two span masonry arch bridge repaired with CFRP plates, demonstrating that FRP repair can significantly improve the structural performance of a single ring masonry arch bridge. The following conclusions can be made from the experimental results:

1. The load capacity of the masonry arch bridge can be significantly enhanced by bonding CFRP strips to the arch's intrados.
2. The load capacity and stiffness of the arch are increased due to the restriction of the intrados crack opening by the CFRP plates.
3. The CFRP repaired masonry arch bridge failed through a combination of cracking within the masonry and brittle debonding along the adhesive joint. Two types of masonry cracks were observed: flexural crack and mixed flexural and shear cracks, and these resulted in flexural crack and shear crack induced debonding of the CFRP from the masonry.
4. The residual strength of the FRP repaired arch after debonding failure can be significantly higher than the original un-repaired arch because the debonded FRP plates form ties to the arch which altered the behaviour of the structure.

ACKNOWLEDGEMENTS

The authors would like to acknowledge the support from the Scottish Funding Council for the Joint Research Institute between the University of Edinburgh and Heriot-Watt University which forms part of the Edinburgh Research Partnership in Engineering and Mathematics (ERPem). They would also like to acknowledge the support from the UK Engineering and Physical Sciences Research Council (EPSRC) and Shell for providing the first author the Dorothy Hodgkin Postgraduate Award. Mr Jim Hutcheson and Mr Derek Jardine are gratefully acknowledged for their technical support throughout the tests.

REFERENCES

1. Valluzzi, M. R., Valdemarca, M. and Modena, C., Behaviour of brick masonry vaults strengthened by FRP laminates. *Journal of Composites for Construction*, 5(3), 163-169 (2001).
2. Foraboschi, P., Strengthening of Masonry Arches with Fiber-Reinforced Polymer Strips. *Journal of Composites for Construction*, 8(3), 191-202 (2004).
3. Bati, S. B., Rovero, L. and Tonietti, U., Strengthening Masonry Arches with Composite Materials. *Journal of Composites for Construction*, 11(1), 33-41 (2007).
4. Lorenzis, L. D., Dimitri, R. and Tegola, A. L., Reduction of the lateral thrust of masonry arches and vaults with FRP composites. *Construction and Building materials*, 21, 1415-14430 (2007).
5. Tao,Y., Stratford, T., Li, X. Q., and Chen, J. F., An experimental investigation into the behaviour of a two span masonry arch bridge repaired with FRP presented at the *9th Fiber-Reinforced Polymer Reinforcement for Concrete Structures*, Sydeny, July 13-15, 2009.
6. Heyman, J., *The masonry arch*. Ellis Horwood limited Publ., 1982.
7. Chen, J. F., Load-capacity of masonry arch bridges strengthened with fibre reinforced polymer composites. *Advances in Structural Engineering*, 5(1), 2002, 37-44.
8. Bati, S. B. and Rovero, L., Towards a methodology for estimating strength and collapse mechanism in masonry arches strengthened with fibre reinforced polymer applied on external surfaces. *Materials and Structures*, 41(7), 2008, 1291-1306.